Structure and Hydride Transfer Mechanism of a Moderate Thermophilic Dihydrofolate Reductase from Bacillus stearothermophilus and Comparison to Its Mesophilic and Hyperthermophilic...

ARTICLE *in* BIOCHEMISTRY · SEPTEMBER 2005

Impact Factor: 3.02 · DOI: 10.1021/bi050630j · Source: PubMed

Structure and Hydride Transfer Mechanism of a Moderate Thermophilic Dihydrofolate Reductase from *Bacillus stearothermophilus* and Comparison to Its Mesophilic and Hyperthermophilic Homologues[†,‡]

Hui Sun Kim,[§] Steven M. Damo,[§] Seok-Yong Lee,[§] David Wemmer,[§] and Judith P. Klinman*[,§,||]

Department of Chemistry and Department of Molecular and Cell Biology, University of California, Berkeley, California 94720-1460

Received April 5, 2005; Revised Manuscript Received May 10, 2005

ABSTRACT: Dihydrofolate reductase (DHFR) from a moderate thermophilic organism, *Bacillus stearothermophilus*, has been cloned and expressed. Physical characterization of the protein (BsDHFR) indicates that it is a monomeric protein with a molecular mass of 18 694.6 Da (0.8), coincident with the mass of 18 694.67 Da calculated from the primary sequence. Determination of the X-ray structure of BsDHFR provides the first structure for a monomeric DHFR from a thermophilic organism, indicating a high degree of conservation of structure in relation to all chromosomal DHFRs. Structurally based sequence alignment of DHFRs indicates the following levels of sequence identity and similarity for BsDHFR: 38 and 58% with *Escherichia coli*, 35 and 56% with *Lactobacillus casei*, and 23 and 40% with *Thermotoga maritima*, respectively. Steady state kinetic isotope effect studies indicate an ordered kinetic mechanism at elevated temperatures, with NADPH binding first to the enzyme. This converts to a more random mechanism at reduced temperatures, reflected in a greatly reduced K_m for dihydrofolate at 20 °C in relation to that at 60 °C. A reduction in either temperature or pH reduces the degree to which the hydride transfer step is rate-determining for the second-order reaction of DHF with the enzyme−NADPH binary complex. Transient state kinetics have been used to study the temperature dependence of the isotope effect on hydride transfer at pH 9 between 10 and 50 °C. The data support rate-limiting hydride transfer with a moderate enthalpy of activation ($E_a = 5.5$ kcal/mol) and a somewhat greater temperature dependence for the kinetic isotope effect than predicted from classical behavior [$A_H/A_D = 0.57$ (0.15)]. Comparison of kinetic parameters for BsDHFR to published data for DHFR from *E. coli* and *T. maritima* shows a decreasing trend in efficiency of hydride transfer with increasing thermophilicity of the protein. These results are discussed in the context of the capacity of each enzyme to optimize H-tunneling from donor (NADPH) to acceptor (DHF) substrates.

A particularly promising approach to understanding the impact of dynamics on protein function is to examine highly homologous proteins that catalyze reactions within widely different temperature ranges (*1*, *2*). It is generally believed that these proteins must achieve a balance between the formation of stable folded structures and the retention of sufficient flexibility for efficient catalysis (*3*, *4*).

The dihydrofolate reductase (DHFR) from mesophilic sources, in particular, *Escherichia coli*, is one of the best-characterized enzymes. The studies on *E. coli* DHFR include the elucidation of the kinetic mechanism as a function of pH (*5*), determination of three-dimensional structures of a range of enzyme−ligand complexes (*6*, *7*), and the demonstration of protein dynamic features that may impact substrate binding and catalysis (*8*−*13*). Site specific mutagenesis studies showed that modification of residues that are both proximal and distal with respect to the active site can impact substrate binding and its conversion to product (*14*−*18*). Computational work has included molecular dynamics simulations in the nanosecond range for both wild-type and mutant enzymes, indicating a reduction in correlated motions for mutant enzymes that leads to higher reaction barriers (*19*, *20*). Simulations by Hammes-Schiffer and co-workers of the quantum transfer of hydride ion from cofactor NADPH to substrate dihydrofolate (DHF), eq 1, show how movements within specific regions of protein can modulate the wave function overlap between the hydride donor and acceptor potential energy wells (*21*).

$$\mathrm{NADPH} + \mathrm{DHF} + \mathrm{H^+} \rightarrow \mathrm{NADP^+} + \mathrm{THF} \qquad (1)$$

where THF is tetrahydrofolate.

In keeping with the growing evidence for a role for quantum mechanical hydrogen tunneling in enzyme-mediated H-transfer processes (*22*, *23*), recent experimental studies by Kohen and co-workers indicate a temperature-independent primary isotope effect in the reduction of DHF by NADPH,

[†] This work was supported by a grant from the Jane Coffin Childs Memorial Fund for Research (JCC-61-1124) to H.S.K., a NSF Predoctoral Fellowship to S.M.D., and grants from the NIH to J.P.K. (GM39296) and to D.W. (GM08295).

[‡] Coordinates have been deposited with the Protein Data Bank as entry 1ZDR.

* To whom correspondence should be addressed. Telephone: (510) 643-5020. Fax: (510) 643-6232. E-mail: klinman@berkeley.edu.

[§] Department of Chemistry.

[||] Department of Molecular and Cell Biology.

10.1021/bi050630j CCC: $30.25
Published on Web 08/05/2005

catalyzed by the *E. coli* DHFR (*24*). These studies, which used multiple labeled substrates and competitive methods, have allowed the extraction of intrinsic kinetic isotope effects, free of kinetic complexity. The absence of a temperature dependence for kinetic isotope effects on elementary H-transfer steps is one of the most powerful indicators of nonclassical behavior. As discussed by Knapp and Klinman, temperature-independent isotope effects cannot be easily explained by a tunneling correction, implicating environmentally mediated hydrogen tunneling mechanisms (*25*).

In an earlier study, Alleman et al. (*26*) had also examined the temperature dependence of the hydride transfer process using a DHFR from the hyperthermophile *Thermotoga maritima*. Despite an only 27% level of sequence identity between the *T. maritima* and *E. coli* enzymes, the X-ray structures of the enzyme subunits are fairly similar (*27*). One important distinction is the finding that the *T. maritima* enzyme forms stable dimers, in contrast to the *E. coli* enzyme that is a functional monomer. The altered quaternary structure may explain the different kinetic properties observed for the *T. maritima* enzyme, where the kinetic isotope effect undergoes a transition from being highly temperature dependent (below 25 °C) to significantly less temperature dependent above 25 °C (*26*). This pattern of behavior had been seen earlier for a thermophilic alcohol dehydrogenase, where changes in catalytic properties show a strong correlation with changes in local protein flexibility (*28*−*30*).

In this work, we describe a full structural and kinetic characterization of a moderate thermophilic DHFR isolated from *Bacillus stearothermophilus*. The *B. stearothermophilus* enzyme is shown to be much closer to the *E. coli* DHFR with regard to its quaternary structure, yet shows catalytic properties for the hydride transfer step that lie between those of the *E. coli* and *T. maritima* enzymes. As has been shown for alcohol dehydrogenases from multiple ecological niches (psychrophilic, mesophilic, and thermophilic), the temperature dependence of kinetic isotope effects for hydrogen transfer may be expected to reflect subtle and often local changes in protein dynamical properties (*31*, *32*).

EXPERIMENTAL PROCEDURES

Materials. All materials were reagent grade unless otherwise noted. DHF was prepared from folic acid and purified by repeated crystallization by the method of Blakley, as previously reported (*33*). [4R-^{2}H]NADPH was synthesized using the method of Jeong and Gready using an NADP$^+$-dependent alcohol dehydrogenase from *Thermoanaerobium brockii* (Sigma) and the substrate 2-propanol-d_8 (Aldrich) at 43 °C and pH 9 (*34*). The labeled product was purified by a modified method of Viola, using the ion exchange chromatography resin AG MP-1 (Bio-Rad) in 0.2 M LiCl and 20 mM 1,3-diaminopropane (pH 8.5) (Aldrich), desalted by gel filtration chromatography using Bio-Gel P-2 resin (fine grade, Bio-Rad) in 20 mM 1,3-diaminopropane (pH 8.5), partially lyophilized to reduce the concentration to ∼15 mM, and then stored in 5 mM dithiothreitol at −80 °C (*35*). The unlabeled product NADPH was synthesized and purified in the same way; however, commercially available, enzymatically synthesized NADPH (Sigma) yielded the same results. The extinction coefficients used for concentration determination were 6.22 mM^{-1} cm^{-1} at 340 nm for NADPH and 28 mM^{-1} cm^{-1} at 340 nm for DHF, in 50 mM Tris (pH 7.5). The concentration of purified *B. stearothermophilus* DHFR (see below) was determined by the method of Pace (*36*), using the calculated extinction coefficient of 25 565 M^{-1} cm^{-1} (1.368 mL mg^{-1} cm^{-1}) in 40 mM Hepes (pH 6.8).

Cloning. The entire sequence of the *E. coli* DHFR gene dyr_Ecoli (sp P00379, 159 nucleotides) was used as a probe to Blast search NCBI's available genomic database of thermophilic eubacteria and archaea using the Blosum62 matrix (*37*). The search pulled up a 483-nucleotide (161-amino acid) fragment with 41% identity, 61% similarity, and 2% gap with respect to the *E. coli* DHFR primary sequence in the unfinished genome of *B. stearothermophilus*, with a score of 123 bits (other hits showed scores of 45 bits or lower). An ORF of 492 nucleotides (164 amino acids) terminated by a TAG stop codon was identified. The sequence was PCR-amplified from a genomic DNA preparation of *B. stearothermophilus* strain 10, a kind gift of B. Roe (Department of Chemistry and Biochemistry, University of Oklahoma, Norman, OK). The primers 5′-GGAATTC-CATATGATTTCGCACATTGTGGCAATGGATGAAAAC-CGG-3′ (forward) and 5′-CGCGGATCCATTATTTCGC-CTTTTTCCGCTCATAAATGATAAAGGC-3′ (reverse) were used to PCR-amplify the putative DHFR gene sequence using standard PCR conditions and an annealing temperature of 60 °C. The amplified product was cloned into the pet21a-(+) vector between the unique NdeI (5′) and BamHI (3′) sites using T4 DNA ligase, and then transformed into competent DH5α cells for subcloning. Purified plasmid from the DH5α transformants was used to transform BL21/DE3 cells for expression using the hexaminecobalt chloride method of Hanahan (Maniatis 1.74) (*38*). The insert was sequenced and verified using the T7 promoter primer.

Recombinant Protein Overexpression and Purification. BL21/DE3 transformants were grown at 37 °C in LB containing 100 μg/mL ampicillin until the OD_{600} reached 0.6, and then the growth temperature was reduced to 30 °C and the expression induced by addition of IPTG to a final concentration of 1 mM. Expression was allowed for 12−14 h at 30 °C. The cells were harvested, washed with 0.9% NaCl, and centrifuged. The cell pellet was resuspended in 40 mM HEPES (pH 6.8) and lysed by sonication. The supernatant from the centrifuged cell extract was heat-precipitated at 55 °C for 20 min and then centrifuged. The resulting supernatant was loaded onto a SP-Sepharose cation exchange column pre-equilibrated in 40 mM HEPES (pH 6.8) and then eluted with a 0 to 1 M NaCl gradient. The pooled DHFR fractions were concentrated in an Amicon concentrator and loaded onto a Superdex 75 prep grade gel filtration column for final purification. The pooled fractions from gel filtration chromatography were concentrated and exchanged into 40 mM HEPES (pH 6.8) for storage at −80 °C.

Molecular Characterizations. The purified protein, from which salt and buffer had been removed by reverse-phase HPLC, was analyzed by electrospray mass spectrometry using a Bruker Esquire-LC mass spectrometer. Size exclusion chromatography was performed using Sephadex G-75 superfine resin (Pharmacia) on a low-pressure column (1 cm inside diameter × 90 cm), with 40 mM HEPES (pH 6.8) and 75 mM NaCl as the elution buffer. The molecular mass standard kit contained protein markers ranging from 6.5 to

66.0 kDa (Sigma MW-GF-70; apoprotein, 6.5 kDa; cytochrome *c*, 12.4 kDa; carbonic anhydrase, 29.0 kDa; albumin, 66.0 kDa). The pI of the protein was determined using the Pharmacia Phast isoelectric focusing system, with a precast gel (PhastGel IEF 3-9, Pharmacia) and pI markers which ranged from pH 3.6 to 8.8 (Sigma).

Sequence Alignment. Coordinates of a representative structure from each organism were taken from the Protein Data Bank (*T. maritima* 1CZ3, *E. coli* 1DRE, *Gallus gallus* 8DFR, *Candida albicans* 1AI9, *Homo sapiens* 2DHF, *Pneumocystis carinii* 1DYR, *Lactobacillus casei* 3DFR, and *Haloferax volcanii* 1VDR). Structure-based sequence alignment was performed using STAMP (*39*), and the figure was generated using the Texshade Package (*40*).

Protein Crystallization and Data Collection. Purified DHFR was concentrated to 10 mg/mL and screened for crystallization conditions (*41*) at 25 °C. Diffraction quality crystals appeared within 1 day from a solution of 0.2 M Tris (pH 7.4) and 1.75 M ammonium sulfate. A cryoprotecting solution was made by adding glycerol to the mother liquor to a final concentration of 22%. Crystals were frozen in liquid nitrogen prior to data collection.

Diffraction data sets to 2.0 Å resolution were collected on a Quantum 210 CCD detector at the Advanced Light Source (Berkeley, CA) on beamlines 8.3.1 and 5.0.2. The detector distance was set to 210 mm, and the wavelength was 1.000 Å. A total of 180 frames were collected with a 1° oscillation scan for a duration of 20 s per frame.

The diffraction data were indexed on the basis of tetragonal space group *P*4212 with the following dimensions: $a = b = 104.65$ Å and $c = 116.37$ Å. There are two molecules in the asymmetric unit corresponding to a solvent content of 69.4%.

Structure Solution and Refinement. The phase was solved by molecular replacement using MOLREP (*42*). The *E. coli* DHFR ternary complex (PDB entry 1RX2) was used as a search model, unliganded and with nonconserved residues mutated to alanine. Molecular packing of alternative solutions was checked manually.

Once the solutions were verified, the model was refined iteratively using several rounds of simulated annealing and temperature factor refinement using CNS (*43*) and model rebuilding using O (*44*) based on $2F_o - F_c$ and $F_o - F_c$ electron density maps. Strict noncrystallographic symmetry (NCS) averaging was used during the initial rounds of refinement. This restraint was later relaxed to account for different conformations of loop regions based on the electron density maps.

Stucture Rendering and Analysis. Graphical representations of the BsDHFR structure were generated using Molscript and Raster3d (*45*, *65*). Secondary structure assignments were made with DSSP (*46*). The model quality was assessed using Procheck (*47*).

Steady State Kinetic Measurements. The initial velocity for the DHFR reaction was determined by measuring the rate of enzyme-dependent decrease at 340 nm using the absorbance change of 13.2 mM^{-1} cm^{-1}. Data were collected on a Hewlett-Packard 8452A diode array spectrophotometer. Standard assay conditions used MTEN buffer [50 mM 2-(*N*-morpholino)ethanesulfonic acid, 25 mM tris(hydroxymethyl)-aminomethane, 25 mM ethanolamine, and 100 mM NaCl] at pH 7, 0.1 mg/mL BSA, 80 μM NADPH, 60 μM DHF, and a DHFR concentration of typically ~1 nM; the assay temperature was 40 °C. The reaction was initiated by the addition of 10 μL of enzyme to a cuvette containing 990 μL of buffer, BSA, NADPH, and DHF, which had been preincubated for 5 min at the appropriate temperature. The order of addition did not influence the catalytic rate under these conditions. In more detailed kinetic studies, the pH, assay temperature, and NADPH, DHF, and DHFR concentrations were varied depending on the experiment; in each instance, the conditions of the experiment are recorded in the legends of the figures. The pH of all buffers was adjusted at the experimental temperature.

Transient State Kinetic Measurements. A Hi-Tech Scientific stopped flow apparatus was used with absorbance monitoring at 340 nm, under single-turnover conditions. NADPH was preincubated with DHFR for 5 min in syringe 1 at the desired temperature in a thermostated syringe compartment, and then the reaction was initiated by rapidly mixing the contents with DHF from syringe 2. Final assay conditions are 20 μM DHFR, 100 μM NADPH(D), and 2.5 μM DHF in MTEN buffer (pH 9), except for the 50 °C data, which required 40 μM DHFR to saturate the DHF due to the partial instability of DHFR at this temperature under these conditions. The kinetic data were analyzed with a single-exponential fit.

RESULTS

Cloning, Overexpression, and Purification. The ORF, consisting of 492 nucleotides (164 amino acids) terminated by a TAG stop codon, was PCR-amplified from a genomic preparation of *B. stearothermophilus* to a single dominant band on an agarose gel, and inserted into a subcloning vector. DNA sequencing verified the insertion of the correct recombinant gene [cf. Figure 1 for the DNA-derived protein sequence of the *B. stearothermophilus* DHFR (BsDHFR) and its structure-based sequence alignment to DHFRs from seven other sources]. The protein product was overexpressed from an *E. coli* pet21a expression system under standard conditions. Although a significant portion segregated into inclusion bodies, soluble DHFR was highly overexpressed, making up approximately 40% of the soluble cell extract (Figure 2). A three-step purification protocol of heat precipitation, cation exchange chromatography, and gel filtration chromatography yielded typically 70 mg of pure protein/L of culture. Due to the high level of overexpression, the enrichment factor was only ~3-fold. The purified product showed a single dominant band by SDS−PAGE and a single peak by analytical reverse-phase HPLC analysis.

Molecular Characteristics. The molecular mass of the purified protein was determined using SDS−PAGE and mass spectrometry. The final purified product showed a single band of ~20 kDa by gel electrophoresis under denaturing conditions (Figure 2). Electrospray mass spectrometry gave a mass of 18 694.6 ± 0.8 Da, coincident with the molecular mass of 18 694.67 Da calculated from the primary sequence. Size exclusion chromatography was performed under neutral conditions and with 75 mM salt to determine the oligomerization state of the native protein; this indicated a molecular mass of ca. 15 000 Da for the DHFR protein, correlating

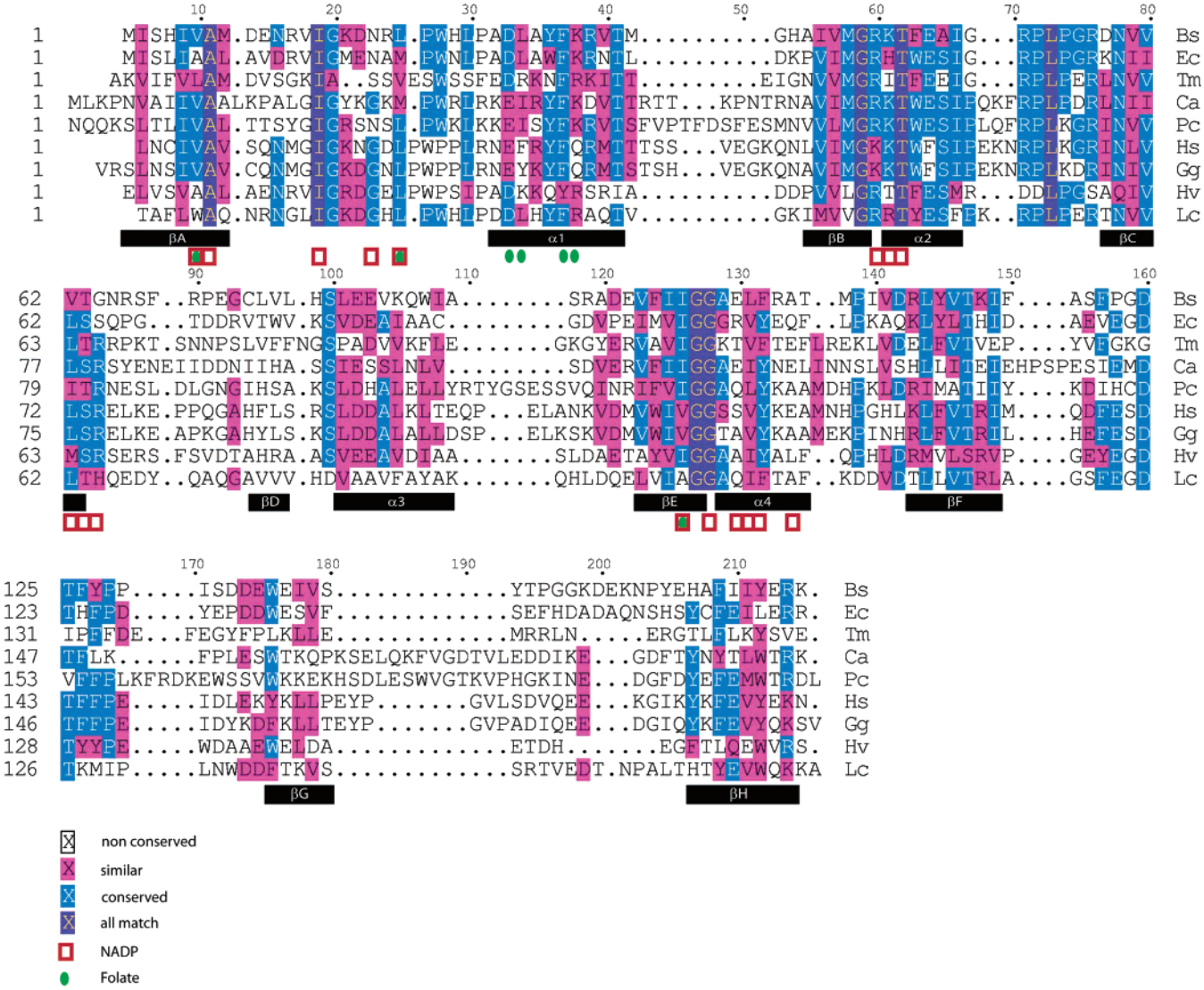

FIGURE 1: Structure-based sequence alignment (*43*) of representative DHFR structures: Bs, *B. stearothermophilus*; Ec, *E. coli*; Tm, *T. maritima*; Ca, *C. albicans*; Pc, *P. carinii*; Hs, *H. sapiens*; Gg, *G. gallus*; Hv, *H. volcanii*; and Lc, *L. casei*. Residues that contact folate or NADP in *E. coli* (1RX2) are indicated (*51*−*53*, *60*−*64*).

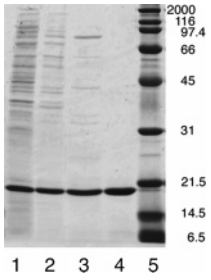

FIGURE 2: SDS−PAGE gel of DHFR purification: (1) supernatant of the cell extract, (2) supernatant of the heat precipitation step, (3) pool of fractions from cation exchange chromatography, (4) pool of fractions from size exclusion chromatography, and (5) molecular mass standards in kilodaltons.

closely with the calculated monomeric mass. Isoelectric focusing indicated a pI of 8.2 for the purified DHFR protein.

Sequence Analysis. Figure 1 shows the structure-based sequence alignment of the DHFR from *B. stearothermophilus* (BsDHFR) with DHFRs from other organisms. The sequences of DHFR across all species are highly conserved. Interestingly, conserved residues span very different amino acid types and include not only those at the active site but also distal residues found in loop regions. This suggests the importance of balancing the structural integrity and dynamic flexibility for the function of the enzyme.

Relative to the other known structures of DHFRs, the sequence of *B. stearothermophilus* shares the greatest sequence identity and similarity with the DHFR from *E. coli* (38 and 58%, respectively), followed by the DHFR from *L. casei* (35 and 56%, respectively). Notably, there is significantly less sequence identity and similarity (23 and 40%, respectively) with the hyperthermophilic DHFR from *T. maritima* (TmDHFR).

Structure Analysis. The three-dimensional structure of BsDHFR, determined by X-ray crystallography, is shown in Figure 3, together with its comparison to the *E. coli* and *T. maritima* enzymes. The structure of BsDHFR is the first monomeric DHFR structure from a thermophilic organism. The apo structure has been determined and refined to a resolution of 2.0 Å. The quality of the model is indicated by a reasonable R factor ($R_{working}$ = 21.0%, and R_{free} = 24.8%) with dihedral angles residing in allowable Ramachandran space (100% in allowed region and 92% in most favored), and clearly interpretable electron density maps. All

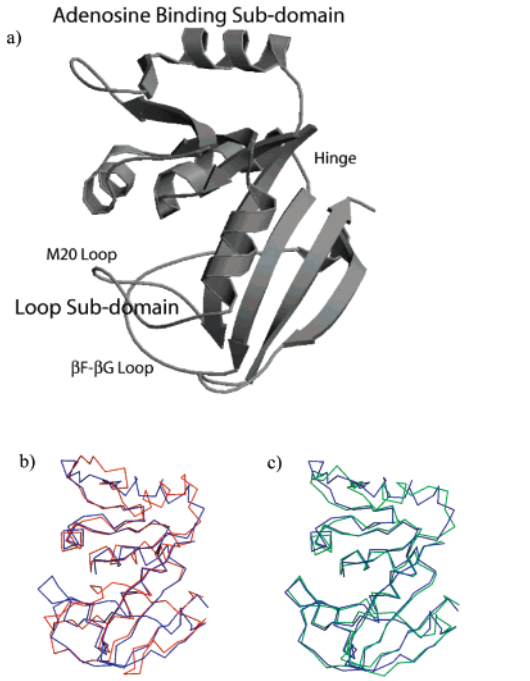

FIGURE 3: (a) Three-dimensional structure of BsDHFR. (b) Overlay of Cα traces of BsDHFR (blue) and TmDHFR (red) monomers. (c) Overlay of Cα traces of BsDHFR (blue) and EcDHFR (green).

residues are well-defined, including side chains in the electron density, except for the last three C-terminal amino acids. As with all chromosomal DHFRs, the structure is highly conserved. The α/β fold is composed of a central eight-stranded (A−H) β-sheet flanked by a pair of α-helices (1−4) on either side. The globular protein is composed of two subdomains, an adenosine-binding subdomain and a loop subdomain.

BsDHFR Activity. A standard assay at 40 °C allowed initial screening of activity as a function of reaction conditions. The dependence of turnover rate on NaCl concentration at neutral pH indicated a ca. 20% increase in activity up to 0.2 M, with activity declining above this salt concentration and falling to zero at 0.8 M NaCl (data not shown). The pH profile under the standard assay condition showed a pK_a of 7.5, with activity decreasing ca. 20-fold at pH 9 (Figure 4). The optimum temperature of activity at pH 7 was determined to be 75 °C, with activity falling off precipitously above this value; at pH 9, the optimal temperature of activity fell to 65 °C (data not shown).

Enzyme stability was examined at pH 6.8 as a function of temperature, showing a very rapid loss of activity in the absence of substrate above 64 °C. At 60 °C, the impact of enzyme concentration, salt, and substrates is illustrated in Figure 5. With the addition of a 5-fold excess of NADPH or DHF, 70−80% of the activity remains after incubation for 1 h at 60 °C.

Noncompetitive Steady State Kinetic Isotope Effects. Michaelis−Menten parameters for the *B. stearothermophilus* DHFR (BsDHFR) at pH 7 and 60 °C, conditions that are expected to approximate the physiological niche of the bacterium, are as follows: k_{cat} = 217 (8) s^{-1}, k_{cat}/K_m(NADPH) = 20.9 (2.5) $\mu M^{-1}\ s^{-1}$, K_m(NADPH) = 10.4 μM, k_{cat}/K_m(DHF) = 58.6 (3.8) $\mu M^{-1}\ s^{-1}$, and K_m(DHF) = 3.7 μM. The properties of deuterium-labeled NADPH were compared to those of the protium cofactor as a function of

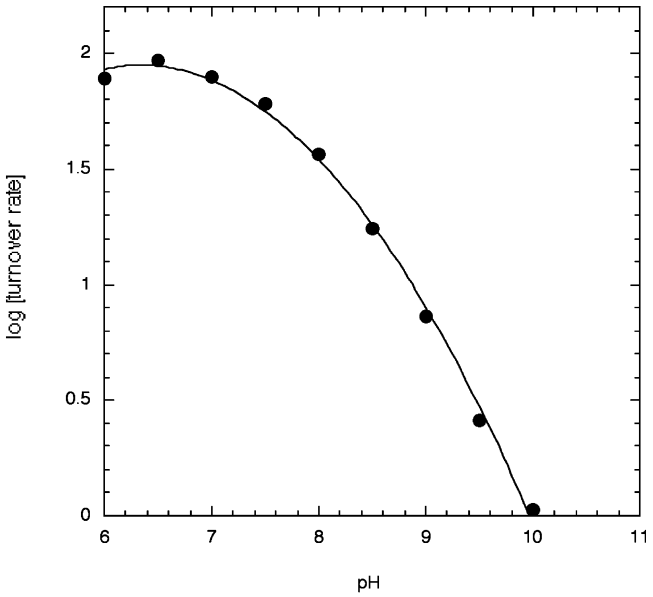

FIGURE 4: pH dependence of DHFR activity, in MTEN buffer at various pH values and 40 °C under otherwise standard conditions.

pH (Figure 6), showing that $^Dk_{cat}/K_m$(DHF) is less than $^Dk_{cat}$ at neutral pH and that both $^Dk_{cat}$ and $^Dk_{cat}/K_m$(DHF) increase to a common value of 2.7 at pH 9. The smaller $^Dk_{cat}/K_m$(DHF) in comparison to $^Dk_{cat}$ at neutral pH suggests that substrate binding is partially rate determining under these conditions. The increase in $^Dk_{cat}$ and $^Dk_{cat}/K_m$ with an increase in pH, coupled with the coincidence of their maximal value at pH 9, supports the view that the hydride transfer step is fully rate limiting at pH 9 (see below). This behavior is concomitant with a decrease in the observed catalytic rate as a function of pH (cf. Figure 4).

Noncompetitive k_{cat}/K_m kinetic isotope effects were subsequently measured at pH 9 as a function of the concentration of the alternate substrate, i.e., $^Dk_{cat}/K_m$(NADPH) as a function of [DHF] and $^Dk_{cat}/K_m$(DHF) as a function of [NADPH]. This examination of isotope effects on k_{cat}/K_m allows for the deduction of a kinetic mechanism in a multireactant enzyme system (*48*, *49*). At 60 °C, the isotope effect determined at a low [DHF], $^D[k_{cat}/K_m(DHF)] \sim 2.7$, is independent of NADPH concentration, while the isotope effect at a low [NADPH(D)], $^D[k_{cat}/K_m(NADPH(D))]$, decreases from ca. 2.2 toward 1 as the DHF concentration increases (Figure 7A). This pattern, in which the $^D(k_{cat}/K_m)$ of one substrate is independent of the cosubstrate concentration while the $^D(k_{cat}/K_m)$ of the alternate substrate reduces toward unity at saturating cosubstrate concentrations, is clearly indicative of a steady state ordered mechanism for substrate binding. Increasing the concentration of the first substrate that binds the enzyme has no effect on the commitment to catalysis in an ordered mechanism, while increasing the concentration of the second substrate drives the initial enzyme−substrate binary complex into the active ternary complex and raises the commitment to catalysis to infinity, thus reducing the k_{cat}/K_m isotope effect to 1. These results show that NADPH is the first substrate to bind, followed by DHF. For both substrates, the limiting isotope effect on k_{cat}/K_m, at the lower cosubstrate concentration, approximates the limiting isotope effect on k_{cat}, at saturating concentrations of both substrates (Figure 7A and Table 1). In agreement with the results from the pH dependence study (Figure 6), the isotopically sensitive

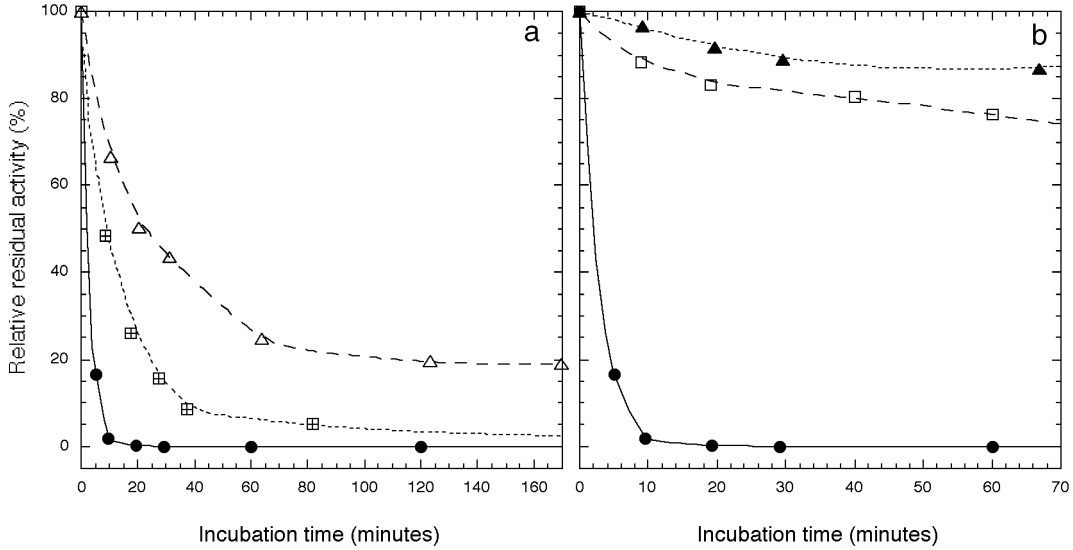

FIGURE 5: (a) Effect of enzyme concentration and NaCl on DHFR stability at 60 °C, under the following incubation conditions: (●) 0.2 mg/mL (10.7 μM) enzyme in 40 mM HEPES (pH 6.8), (⊞) 0.05 mg/mL (2.68 μM) enzyme in 40 mM HEPES (pH 6.8), and (△) 0.2 mg/mL enzyme in 40 mM HEPES (pH 6.8) and 0.2 M NaCl. (b) Effect of NADPH and DHF on DHFR stability at 60 °C at 0.2 mg/mL enzyme and in 40 mM HEPES (pH 6.8) under the following incubation conditions: (●) no additions, (□) with 100 μM NADPH, and (▲) with 100 μM DHF. Aliquots were removed after the indicated incubation time period to measure the residual activity under standard assay conditions.

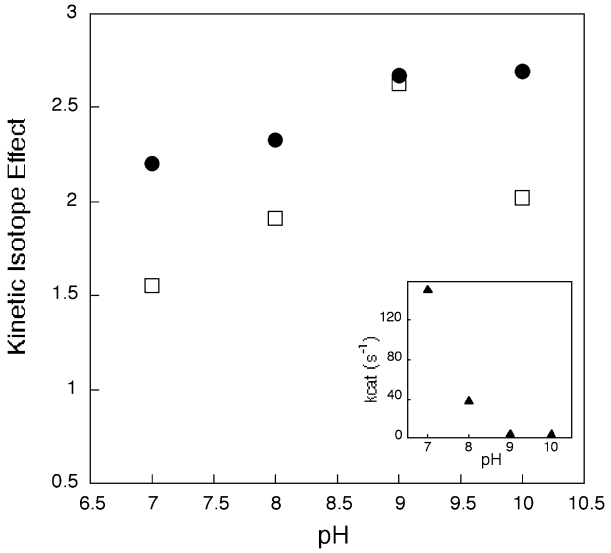

FIGURE 6: pH dependence of deuterium kinetic isotope effects at 60 °C: $^{D}k_{cat}$ (●) and $^{D}k_{cat}/K_m$(DHF) (□). Assay conditions are 0.8−80 nM DHFR, 25 μM NADPH(D) [100 μM NADPH(D) yielded similar results], and 1.25−100 μM DHF in MTEN buffer with the appropriate pH with 0.1 mg/mL BSA. The inset shows the pH dependence of the DHFR turnover rate.

hydride transfer step is concluded to be rate-determining for k_{cat} and k_{cat}/K_m(DHF) at 60 °C and pH 9.

The isotope effects as a function of the cosubstrate concentration show a different pattern at 20 °C (Figure 7B). At this lower temperature, $^{D}k_{cat}/K_m$(DHF) appears to slightly decrease with an increase in NADPH concentration from ca. 2.4 to 2, while $^{D}k_{cat}/K_m$(NADPH) appears to remain independent of the DHF concentration, at ca. 1.1. This pattern, in which saturation by one substrate will reduce but not abolish the k_{cat}/K_m isotope effect of the other substrate, is indicative of a steady state random component to the mechanism. The observation that $^{D}k_{cat}/K_m$(NADPH) appears to be independent of the cosubstrate concentration and is very close to unity suggests that DHF saturates at a very low concentration such that possible trends in $^{D}k_{cat}/K_m$(NADPH) are obscured. The lower value for the apparent $^{D}k_{cat}/K_m$(NADPH) (∼1.1) in comparison to the apparent $^{D}k_{cat}/K_m$(DHF) (∼2) at a saturating cosubstrate concentration further indicates that while the mechanism is random, there is still a preferred order of NADPH binding first. At 20 °C, the limiting $^{D}k_{cat}/K_m$ value for DHF is lower than the $^{D}k_{cat}$ of 3.2, once again pointing toward partial rate limitation by substrate binding. A reduction in either pH (Figure 6) or temperature (Figure 7) reduces the extent to which chemistry is rate-limiting for the second-order reaction of DHF with the enzyme−NADPH binary complex.

Hydride Transfer at Variable Temperatures. To study the temperature dependence of the hydride transfer step, we turned to the use of transient state kinetics at variable temperatures. Single-turnover conditions were applied in which NADPH is prebound to the enzyme at a concentration that is sufficiently high to saturate the available, limiting DHF. The data in Figure 8 indicate that a ratio of NADPH to enzyme slightly greater than unity and a ratio of enzyme to DHF of 5−10 led to optimal turnover rates at low and elevated temperatures. The final first-order rate constants using NADPH and NADPD between 10 and 50 °C are shown in Figure 9a, with the temperature dependence of the isotope effects in Figure 9b. The resulting Arrhenius parameters have been summarized in Table 2. The data show that, in contrast to results for the highly homologous *E. coli* DHFR, the isotope effects are temperature-dependent and yield an isotope effect on the Arrhenius prefactor that falls below unity.

DISCUSSION

General Properties of the BsDHFR. The identification and cloning of the BsDHFR were aided by its high degree of similarity to the *E. coli* DHFR gene. The level of protein expression in *E. coli* was very high, and the initial heat precipitation step both allowed for the ready separation of the BsDHFR from its host DHFR and provided a large degree of the purification. The subunit molecular mass for BsDHFR

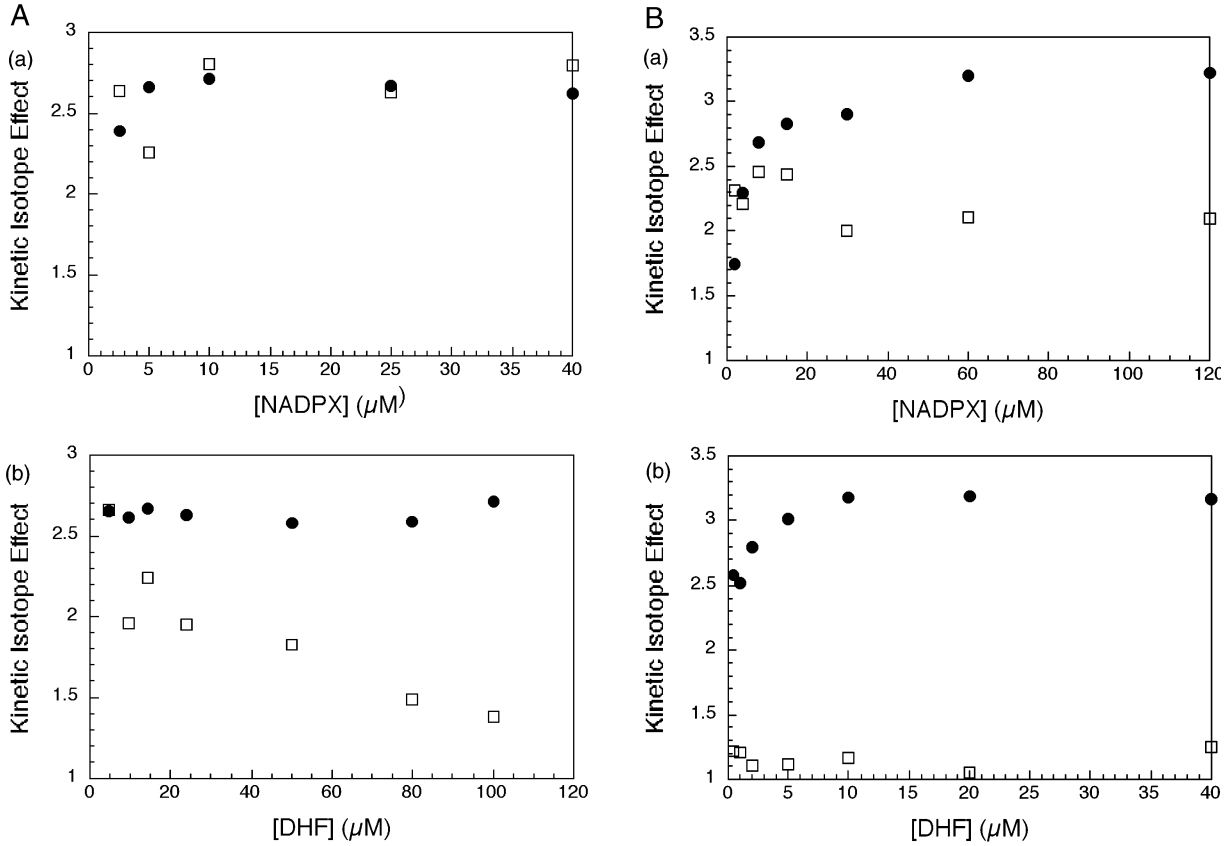

FIGURE 7: (A) Dependence of deuterium kinetic isotope effects on cosubstrate concentration at 60 °C. (a) KIE as a function of NADPH(D) concentration at saturating DHF (●) and at low DHF (□) concentrations. (b) KIE as a function of DHF concentration at saturating NADPH-(D) (●) and at low NADPH(D) (□) concentrations. Typically, 30−35 nM enzyme was used in MTEN buffer (pH 9). (B) Dependence of kinetic isotope effects on cosubstrate concentration at 20 °C. (a) KIE as a function of NADPH(D) concentration at saturating DHF (●) and at low DHF (□) concentrations. (b) KIE as a function of DHF concentration at saturating NADPH(D) (●) and at low NADPH(D) (□) concentrations. Typically, 25−65 nM enzyme was used in MTEN buffer (pH 9).

Table 1: Steady State Kinetic Parameters and Isotope Effects for *B. stearothermophilus* DHFR at pH 9 and 60 or 20 °C[a]

	60 °C					20 °C				
substrate	k_{cat} (s^{-1})	K_m (μM)	k_{cat}/K_m (μM^{-1} s^{-1})	$^Dk_{cat}$	$^D(k_{cat}/K_m)$	k_{cat} (s^{-1})	K_m (μM)	k_{cat}/K_m (μM^{-1} s^{-1})	$^Dk_{cat}$	$^D(k_{cat}/K_m)$
NADPH	4.7	2.8	1.7	2.7	2.7	2.2	3.5	0.6	3.2	1.1
DHF	4.9	12.3	0.4	2.7	2.7	2.3	1.5	1.5	3.2	2.4

[a] Initial velocity assays were carried out using 25−65 nM DHFR in MTEN buffer adjusted to pH 9 at the appropriate temperature, using saturating concentrations ($\geq 10K_m$) of both substrates (k_{cat}) or the cosubstrate (k_{cat}/K_m). Kinetic isotope effects are the limiting values estimated from Figure 7A (60 °C) and Figure 7B (20 °C).

of 18 700 Da, as confirmed by mass spectrometry, is similar to those of other characterized bacterial DHFRs. Unlike the quaternary structure for the hyperthermophilic DHFR from *T. maritima*, the moderate thermophile BsDHFR is monomeric; additionally, though the pI for BsDHFR is elevated to 8.2, it is not as extremely basic (pI >10) as for the *T. maritima* enzyme. The optimal temperature for BsDHFR activity is elevated by approximately 10 °C in relation to the optimal temperature of growth for the organism, which is 65 °C. Preincubation of enzyme indicates a thermostability that coincides with the optimal growth temperature. High salt has an impact on the protein, with activity peaking at 0.2 M and then falling off rapidly at higher ionic strengths.

Steady State Kinetic Characterization. The *B. stearothermophilus* DHFR shows the following steady state kinetic properties. (i) At 60 °C, a temperature close to the optimal growth temperature of the organism, the maximal kinetic isotope effect is 2.7 for both $^Dk_{cat}$ and $^Dk_{cat}/K_m$(DHF) at pH 9. Transient state kinetics, using conditions which isolate the hydride transfer step, also give a k_H/k_D value of 2.7 at the close temperature of 50 °C (see Nature of Hydride

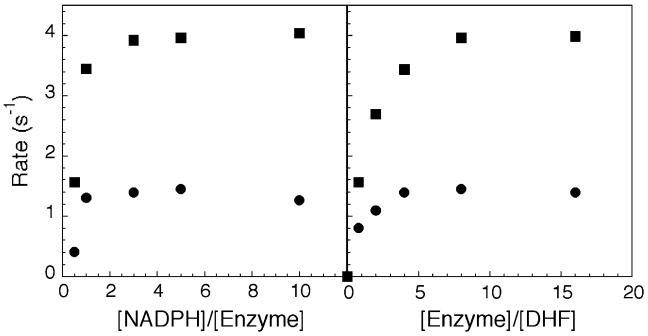

FIGURE 8: Saturation curves for transient kinetics experiments, at 10 (●) and 40 °C (■). The DHF concentration was fixed at 2.5 μM; DHFR and NADPH concentrations were varied to obtain the appropriate ratios. The reaction was initiated by the rapid mixing of DHF to a solution of DHFR and NADPH, in MTEN buffer (pH 9).

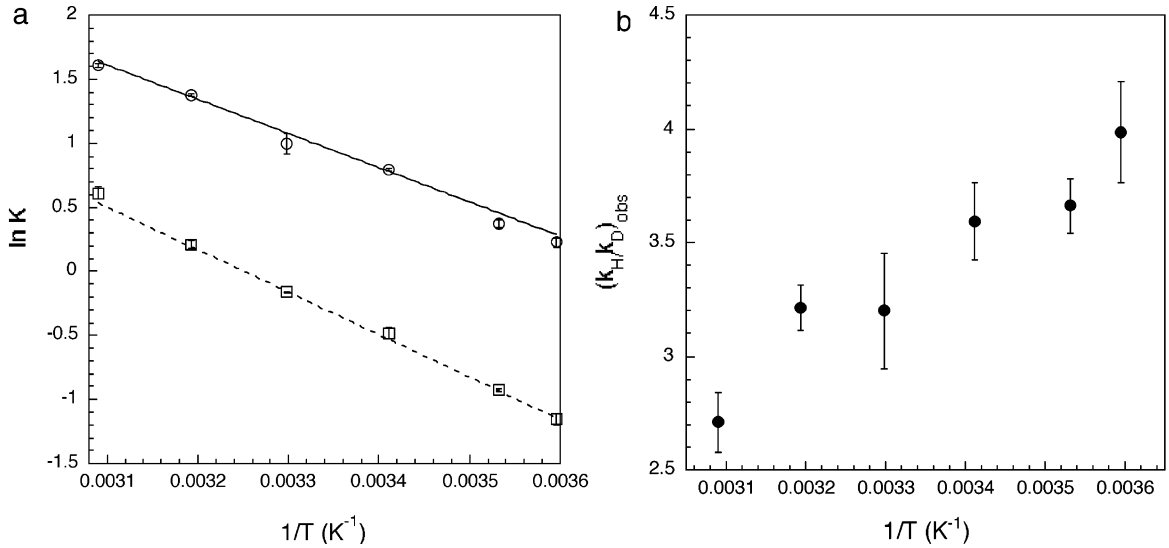

FIGURE 9: (a) Arrhenius plot of DHFR activity as determined by transient state kinetics, using NADPH (○) and NADPD (□) as substrates. The reaction was initiated by the rapid mixing of DHF to a solution of DHFR and NADPH. Final assay conditions are 20 μM DFHR (except at 50 °C, which required 40 μM DHFR to saturate the DHF), 100 μM NADPH(D), and 2.5 μM DHF in MTEN buffer (pH 9). (b) Temperature dependence of kinetic isotope effect as determined by transient kinetics, using NADPH and NADPD as substrates. See the description for panel a for assay conditions.

Table 2: Arrhenius Parameters Derived from Transient State Kinetics

	A	A_H/A_D	E_a (kcal/mol)	$E_{a_D} - E_{a_H}$ (kcal/mol)
H	2.8×10^4 (6×10^3)		5.5 (0.1)	
D	4.9×10^4 (8×10^3)		6.6 (0.1)	
		0.57 ± 0.15		1.1 ± 0.2

Transfer Chemistry). (ii) The contribution of the hydride transfer step to k_{cat} and k_{cat}/K_m(DHF) is pH-dependent under steady state conditions, becoming less rate-limiting as the pH is lowered from 9 to 7. (iii) The kinetic mechanism for substrate addition at 60 °C and pH 9 is ordered with NADPH binding to the enzyme prior to DHF.

There are changes in the steady state kinetics of the enzyme at pH 9 when the temperature is reduced from 60 to 20 °C, with regard to the order of substrate binding and the degree of rate limitation of the hydride transfer step. At 20 °C, the kinetic mechanism has become somewhat random (although the preferred order remains one in which NADPH binds first), and the hydride transfer step is no longer fully rate limiting for k_{cat}/K_m(DHF) (Figure 7B). The pattern of k_{cat}/K_m isotope effects as a function of the cosubstrate concentration suggests that the randomness arises from tighter binding of DHF at the lower temperature. This observation is supported by the significant decrease in the K_m value of the DHF at the lower temperature, from 12.3 μM at 60 °C to 1.5 μM at 20 °C.

The *B. stearothermophilus* DHFR shares a number of kinetic features with DHFRs from other bacterial sources. As in the cases of the mesophilic systems *E. coli* and *L. casei* at 20−25 °C, the *B. stearothermophilus* DHFR at 60 °C displays a rate of hydride transfer chemistry that is pH-dependent, only becoming rate-limiting for all parameters at elevated pH values (*5*, *50*). Reducing the temperature to 25 °C leads to an isotope effect of 3.2, close to the maximal isotope effects of 3 and 3.2 observed for the *E. coli* (*5*) and *L. casei* (*50*) DHFRs, respectively, at 20−25 °C and to the value of ca. 4 observed for TmDHFR, also at 25 °C (*26*). The relatively weak isotope effect appears to be an intrinsic feature of hydride transfer chemistry catalyzed by DHFRs, as well as other dehydrogenases.

The order of substrate binding also resembles that of the mesophilic DHFRs. For both *E. coli* and *L. casei* DHFRs at their physiological temperature, the kinetic mechanism is observed to be a preferred pathway in which NADPH binds first, under saturating NADPH conditions (*5*, *50*). This preference for substrate binding order arises from the feature that THF dissociation is faster from the E−NADPH−THF complex than from the E−THF complex; thus, THF release preferentially occurs after NADPH replaces $NADP^+$ in the E−$NADP^+$−THF ternary product complex. One distinction for BsDHFR is its strictly ordered kinetic mechanism at its physiological temperature of 60 °C (Figure 7A).

Sequence and Structural Analysis. Figure 1 shows the structure-based sequence alignment of BsDHFR with DHFR structures deposited in the Protein Data Bank. The entire alignment underscores the conservation of the DHFR fold (rmsd = 1.27 Å relative to *E. coli*). The structural differences seen are largely due to insertions of amino acids in loop regions. TmDHFR is the one known exception with an entirely different quaternary structure; nevertheless, its monomeric structure remains highly homologous to that of other DHFRs.

The BsDHFR structure aligns well with both the mesophilic *E. coli* (EcDHFR) and hyperthermophilic *T. maritima* (TmDHFR) structures. The BsDHFR structure is most similar to *E. coli* (1.06 Å rmsd based on a pairwise alignment). All elements of secondary structure are superimposable except for helix 3, which in BsDHFR has a 20° tilt relative to that in *E. coli* which is attributed to crystal packing interactions.

As with all DHFRs, the conserved Gly98 and Gly99 adopt a cis conformation; this region is important for binding NADPH. A sulfate ion is present in the cofactor pocket, which is not surprising since sulfate is similar to phosphate and present in excess in the crystallization buffer. A sulfate ion was also seen in a similar position in the TmDHFR structures (*27*).

Kraut and co-workers (*6*, *51*−*53*) have characterized many different conformations of EcDHFR at atomic resolution. Complexes analogous to all kinetic intermediates, including the holoenzyme, the Michaelis complex, the transition state, and the ternary product complex, have been solved. EcDHFR is known to undergo a series of conformational changes as it progresses through the catalytic cycle. Upon ligand binding, the most dramatic conformational changes occur in the M20 loop, which opens and closes over and occludes the active site. Residue Glu17, for example, moves almost 10 Å from the open to occluded conformations. Several NMR studies have examined the role of the M20 loop in substrate binding and product release (*9*, *13*, *54*).

Despite the absence of ligand, the M20 loop in BsDHFR is in the closed conformation (*E. coli* is the only monomeric DHFR that has had the M20 loop crystallized in both the occluded and open conformations). As with other closed DHFR structures, the temperature factors are relatively high for the residues in the M20 loop, an indication of its flexibility. In the TmDHFR, the M20 loop is trapped in a unique open conformation due to packing at the dimer interface (*27*).

Other loop regions throughout the protein undergo comparatively small conformational changes (typically on the order of 1 Å) upon ligand binding. The GF loop, for example, serves to make contacts to the M20 loop in the closed state (*51*). This loop in BsDHFR is also largely similar to the *E. coli* closed conformation.

Comparison of BsDHFR to EcDHFR: Structural Basis of Increased Thermostability. Several studies have attempted to outline the basis of stability of thermophiles versus their mesophilic counterparts (*55*, *56*). On a per protein basis, the differences at the structural level are often subtle, although there are mechanisms that by consensus can contribute to thermostability. Some of these known factors include insertion of prolines, extension of secondary structural elements, the introduction of helix-capping residues, and the addition of salt bridges.

In a comparison of the thermophilic BsDHFR to EcDHFR, it is not immediately obvious what features impart thermostability. Many of the typical factors that contribute to the stability of thermophiles are not apparent in the case of BsDHFR. For example, there are no helix-capping residues, or additional salt bridges or clusters of salt bridges. It is likely that the increased stability of BsDHFR relative to EcDHFR is due to a number of subtle factors. Some suggestions are provided below.

One possible contributor to the thermostability of BsDHFR is the elongation of some secondary structural elements. Helix 3 is longer by two residues. Additionally, β-strands B, C, and E are longer by one to three residues in BsDHFR. The increased secondary structure content in β-strand B is notable, because it includes the conserved residue Met42 that has been shown to be involved in motions that are correlated to hydride transfer. Although these are not substantial increases in secondary structure, they may contribute to stabilizing BsDHFR at higher temperatures.

The insertion of prolines in loop regions that connect secondary structural elements inhibits the flexibility of loop regions, thus stabilizing structure (*57*). There are 11 prolines in BsDHFR (10 in EcDHFR); 6 of the 11 are conserved. Notably, the nonconserved prolines in EcDHFR are in regions of secondary structure that are elongated in BsDHFR (specifically, β-strands B and E). Prolines which may increase stability in BsDHFR can be found in the βG−βH loop and the βC−βD loop. Studies by Benkovic and co-workers (*15*) have shown that the loop containing Gly121 is important for hydride transfer. In BsDHFR, there is a pair of prolines that flank this region which could conceivably affect catalysis by hindering the flexibility of this loop.

A previous study showed the major determinant of stability of the hyperthermophilic DHFR from *T. maritima* is its oligomerization state. TmDHFR is a functioning dimer. Comparison of the monomer subunits of TmDHFR with EcDHFR did not reveal any major structural differences, similar to our comparison here between BsDHFR and EcDHFR. Many of the structural differences observed were due to insertions of a few amino acids or unique conformations of loop regions which are largely involved in the dimer interface in TmDHFR.

Implications of Structure for Catalysis. The consensus is that subtle adaptations in thermophiles serve both to rigidify structure and to allow for optimal function at elevated temperatures. It is important to make clear that these structural adaptations are expected to be propagated into dynamical features (cf. 2). It is interesting that there is no clear determinant of thermostability for BsDHFR relative to the mesophile, yet kinetically its behavior lies between the mesophile and hyperthermophile. Even in the case of the dimeric TmDHFR, its monomeric structure is largely similar to all known DHFR structures. One possible explanation for the decreasing k_{cat} for hydride transfer and increasing involvement of protein gating modes (see Nature of Hydride Transfer Chemistry), as DHFR adapts to higher temperatures, is a decrease in protein flexibility. In *T. maritima*, the catalytically important motions may be largely impaired by dimerization, especially since many of the loop regions are impacted at the dimer interface. The result is that the thermophilic DHFRs are able to function at higher temperatures, albeit at the cost of flexibility.

Kern and co-workers have recently compared the temperature dependence of mesophilic and thermophilic adenylate kinases using NMR (*58*). Their results showed that the flexibility of the loop region that controls product release was greatly reduced in the thermophilic enzyme at ambient temperatures. This flexibility was restored with an increase in the temperature toward the optimum growth temperature of the organism. Although this type of motion is not directly correlated to catalysis, it provides direct evidence for the reduced flexibility of thermophiles as compared to their mesophilic counterparts. In the case of DHFR, the evidence suggests that reduced flexibility affects motions that are linked to hydride transfer efficiency.

Nature of Hydride Transfer Chemistry. A major goal of this study has been to characterize, both structurally and kinetically, a moderately thermophilic DHFR, in particular, the nature of the hydride transfer step and its relationship to protein structure. Previous studies have already provided detailed structural and kinetic data for a mesophilic and hyperthermophilic DHFR that include the temperature dependence of the primary deuterium kinetic isotope effect (KIE) (*24*, *26*). The findings presented herein for a moderate thermophilic DHFR provide a full scale of behaviors for enzymes that function near room temperature (*E. coli*

Table 3: Comparison of Parameters that Characterize the Hydride Transfer Step in the EcDHFR, BsDHFR, and TmDHFR Reactions

enzyme	k_{cat} at pH 9 (s^{-1})[d]	E_a (kcal/mol)	A_H/A_D	k_H/k_D[e]
EcDHFR[a]	16 (25 °C)	3.0	4.0 (1.5)	3.4
BsDHFR[b]	4.8 (60 °C)	5.5	0.57 (0.15)	3.4
TmDHFR[c]	0.62 (80 °C)	12 (<25 °C)	0.002 (0.001) (<25 °C)	3.5
		13 (>25 °C)	1.56 (0.47) (>25 °C)	

[a] From ref *24*. [b] From this study. [c] From ref *26*. [d] Note that differences become exaggerated when k_{cat} is compared at 25 °C for the three enzymes. [e] These values are at 25 °C, with the exception of that of TmDHFR, which is at 40 °C.

DHFR), near 100 °C (*T. maritima* DHFR), and at 65 °C (BsDHFR).

As shown for a significant and growing number of enzyme reactions, including those that catalyze transfer of hydride from reduced nicotinamide cofactor to substrate, the temperature dependence of the KIE is different from that predicted for classical behavior in which $A_H/A_D \sim 1$. In all current models for these deviations, hydrogen tunneling emerges as the primary factor. Increasingly, the temperature dependence of the KIE is found to be more variable than either the rate of hydrogen transfer or the size of the KIE at a single temperature, with A_H/A_D being highly sensitive to changes in temperature, site specific mutations, and modification of the protein surface (see below). Existing models for the origin of the deviant temperature dependencies stress the importance of the initial distance between the donor and acceptor atoms and the nature of the coupling of protein vibrational modes into the hydrogen transfer coordinate (*25*, *59*).

Because the steady state kinetic isotope effect data for BsDHFR showed the possibility of changes in mechanism as a function of temperature, single-turnover conditions capable of isolating the hydride transfer step were used to study the temperature dependence of the hydride transfer chemistry. Under single-turnover conditions in which the NADPH is prebound to the enzyme and the reaction is initiated with a limiting concentration of DHF, an ordered mechanism is imposed and substrate binding kinetics is not rate-limiting. Although the steady state data indicated a temperature optimum of 65 °C, stopped flow data were restricted to ≤50 °C, due to the time needed for incubation of solutions in the stopped flow and the possibility of some alteration of the protein behavior due to temperature-induced unfolding and denaturation.

The fitting of the data in Figure 9 for BsDHFR has been summarized in Table 2, showing a moderate value for E_a and a temperature dependence of the KIE that lies just outside the lower limit for semiclassical behavior. At this juncture, detailed properties of the hydride transfer step are available for BsDHFR, TmDHFR, and EcDHFR, allowing a comparison of the fundamental parameters that determine a hydrogen transfer step for enzymes evolved to function at ca. 25, 65, and 80 °C, respectively (Table 3). Two features emerge immediately from this comparison. First, as pointed out above, the magnitude of the KIE at 25 °C is almost identical among the three proteins, and second, the rates and E_a values are much closer for Ec- and BsDHFR than TmDHFR.

It is now well established that the FG loop of EcDHFR is mobile and undergoes a conformational change in the course of catalysis. In the case of the TmDHFR, this loop is located at the dimer interface, which is expected to decrease loop mobility and increase the barrier to catalysis. It is tempting to attribute the 2−4-fold increase in E_a for TmDHFR as arising from structural changes that must precede the hydrogen transfer and alter the position of the immobilized F−G loop seen in the X-ray structure to one that is capable of increased motion. In this instance, the hydride transfer can be conceptualized as a two-step process, involving a preequilibrium protein isomerization (with a positive $\Delta H°$ value) and a subsequent movement of hydride from the donor (NADPH) to acceptor (DHF) atoms such that $\Delta H^{‡} = \Delta H° + \Delta H^{‡'}$.

In many ways, the most interesting aspect of the collective data in Table 3 is the large difference in the temperature dependence of the KIE that occurs despite little change in the magnitude of the KIE itself. The largest deviations from semiclassical behavior are seen for EcDHFR where $A_H/A_D \gg 1$ and the TmDHFR at a reduced temperature, where $A_H/A_D \ll 1$. In the context of these observations, it is reasonable to assume H-tunneling in all forms of DHFR with differences in the isotope effect on the Arrhenius prefactors arising from changes in the properties of the E−S complex that affect the efficiency of hydrogen transfer.

In a recent treatment of the hydrogen atom transfer catalyzed by soybean lipoxygenase, Hammes-Schiffer and co-workers (*59*) have interpreted changes in the temperature dependence of KIEs largely in the context of changes in the initial distance ($R°$) between donor and acceptor atoms. One consequence of this model is the prediction of significant increases in the magnitude of the KIE as $R°$ increases, contrasting with the behavior of the three DHFRs summarized herein. In an analogous though simpler model, Knapp et al. (*25*) have proposed that differences in protein packing may give rise to subtle changes in the frequency of a fundamental protein motion(s) that controls the sampling of distances between the donor and acceptor atoms, and that changes in this motion (ω_x) can alter the magnitude of A_H/A_D without significantly altering the magnitude of the KIE itself. It is important to point out that significant differences may exist in the degree of (electronic and vibronic) coupling occurring between donor and acceptor atoms in the SLO-1 and DHFR reactions such that the nonadiabatic treatment developed for SLO-1 cannot be directly applied to the movement of charge that occurs in the DHFR reaction. Nonetheless, it seems likely that a difference in protein flexibility, which alters ω_x, is one of the factors contributing to the differences in A_H/A_D observed among the three DHFRs.

In an increasing number of studies, a trend has been observed whereby the magnitude of A_H/A_D is observed to be greater than or close to unity under optimal conditions for a particular enzyme system and, further, to become increasingly inverse as the function of the enzyme becomes compromised. In published works, this type of behavior has been reported for a moderately thermophilic alcohol dehydrogenase at high and low temperatures, for SLO-1 in WT enzyme versus active site mutants, and in glucose oxidase using an enzyme that has undergone different degrees of surface modification away from its native form. The trend is repeated in Table 3, where it can be seen that the value of A_H/A_D declines in a regular fashion from the most efficient enzyme, EcDHFR, to the least efficient enzyme, TmDHFR

below 25 °C. As the number of characterized systems increases, it has become apparent that the sensitivity of kinetic hydrogen isotope effects to temperature may offer a unique glimpse into details of H-transfer coordinates that is simply unavailable from other probes. On the basis of the aggregate available data, we postulate that optimized enzyme systems facilitate reaction of exceptionally well positioned substrates and that perturbations away from this "ideal state" enhance the role of distance sampling, which appears as reduced values for A_H/A_D in enzyme-catalyzed H-transfer.

Future challenges include the continuing development of analytical expressions that allow us to understand the precise factors that control the temperature dependence of the KIE in both adiabatic and nonadiabatic systems, as well as understanding of the protein structural bases for changes in behavior. The availability of X-ray structures for all three of the DHFRs offers a starting point for investigations of differences in protein dynamics using both experimental (NMR and H−D exchange) and computation (molecular dynamics) methodologies.

ACKNOWLEDGMENT

We gratefully acknowledge Jamie Geier for assisting with the initial characterization and Dr. Bruce Roe for providing and checking the BsDHFR gene. Dr. Ho Cho is thanked for helpful discussions and advice. The Advanced Light Source is supported by the Director, Office of Science, Office of Basic Energy Sciences, Materials Sciences Division of the U.S. Department of Energy under Contract DE-AC03-76SF00098 at Lawrence Berkeley National Laboratory (Berkeley, CA).

REFERENCES

1. Kohen, A., Cannio, R., Bartolucci, S., and Klinman, J. P. (1999) Enzyme dynamics and hydrogen tunneling in a thermophilic alcohol dehydrogenase, *Nature 399*, 496−499.
2. Liang, Z. X., Lee, T., Resing, K. A., Ahn, N. G., and Klinman, J. P. (2004) Thermal-activated protein mobility and its correlation with catalysis in thermophilic alcohol dehydrogenase, *Proc. Natl. Acad. Sci. U.S.A. 101*, 9556−9561.
3. Zavodszky, P., Kardos, J., Svinger, A., and Petsko, G. A. (1998) Adjustment of conformational flexibility is a key event in the thermal adaptation of protein, *Proc. Natl. Acad. Sci. U.S.A. 95*, 7406−7411.
4. Somero, G. N., and Siebenaller, J. F. (1979) Inefficient lactate dehydrogenases of deep-sea fishes, *Nature 282*, 100−102.
5. Fierke, C. A., Johnson, K. A., and Benkovic, S. J. (1987) Construction and evaluation of the kinetic scheme associated with dihydrofolate reductase from *Escherichia coli*, *Biochemistry 26*, 4085−4092.
6. Matthews, D. A., Alden, R. A., Bolin, J. T., Freer, S. T., Hamlin, R., Xuong, N., Kraut, J., Poe, M., Williams, M., and Hoogsteen, K. (1977) Dihydrofolate reductase: X-ray structure of the binary complex with methotrexate, *Science 197*, 452−455.
7. Schnell, J. R., Dyson, J., and Wright, P. E. (2004) Structure, dynamics and catalytic function, *Annu. Rev. Biophys. Biomol. Struct. 33*, 119−140.
8. Yang, Q. X., Huang, F. Y., Lin, T. H., Gelbaum, L., Howell, E. E., and Huang, T. H. (1996) Dynamics of trimethoprim bound to dihydrofolate reductase: A deuterium NMR study, *Solid State Nucl. Magn. Reson. 7*, 193−201.
9. Falzone, C. J., Wright, P. E., and Benkovic, S. J. (1994) Dynamics of a flexible loop in dihydrofolate reductase from *Escherichia coli* and its implication for catalysis, *Biochemistry 33*, 439−442.
10. Farnum, M. F., Made, D., Howell, E. E., Hirai, J. T., Warren, M. S., Grimsley, J. K., and Kraut, J. (1991) Analysis of hydride transfer and cofactor fluorescence decay in mutants of dihydrofolate reductase: Possible evidence for participation of enzyme molecular motions in catalysis, *Biochemistry 30*, 11567−11579.
11. Sawaya, M. R., and Kraut, J. (1997) Loop and subdomain movements in the mechanism of *Escherichia* coli dihydrofolate reductase: Crystallographic evidence, *Biochemistry 36*, 586−603.
12. Osborne, M. J., Schnell, J., Benkovic, S. J., Dyson, H. J., and Wright, P. E. (2001) Backbone dynamics in dihydrofolate reductase complexes: Role of loop flexibility in the catalytic mechanism, *Biochemistry 40*, 9846−9859.
13. Schnell, J. R., Dyson, H. J., and Wright, P. E. (2004) Effect of cofactor binding and loop conformation on side chain methyl dynamics in dihydrofolate reductase, *Biochemistry 43*, 374−383.
14. Miller, G. P., and Benkovic, S. J. (1998) Strength of an interloop hydrogen bond determines the kinetic pathway in catalysis by *Escherichia coli* dihydrofolate reductase, *Biochemistry 37*, 6336−6342.
15. Cameron, C. E., and Benkovic, S. J. (1997) Evidence for a functional role of the dynamics of glycine-121 of *Escherichia coli*. Dihydrofolate reductase obtained from kinetic analysis of a site-directed mutant, *Biochemistry 36*, 15792−15800.
16. Miller, G. P., and Benkovic, S. J. (1998) Deletion of a highly motional residue affects formation of the Michaelis complex for *Escherichia coli* dihydrofolate reductase, *Biochemistry 37*, 6327−6335.
17. Agarwal, P. K., Billeter, S. R., Rajagopalan, P. T. R., Benkovic, S. J., and Hammes-Schiffer, S. (2002) Network of coupled promoting motions in enzyme catalysis, *Proc. Natl. Acad. Sci. U.S.A. 99*, 2794−2799.
18. Rajagopalan, P. T., Lutz, S., and Benkovic, S. J. (2002) Coupling interactions of distal residues enhance dihydrofolate reductase catalysis: Mutational effects on hydride transfer rates, *Biochemistry 41*, 12618−12628.
19. Rod, T. H., Radkiewicz, J. L., and Brooks, C. L., III (2003) Correlated motion and the effect of distal mutations in dihydrofolate reductase, *Proc. Natl. Acad. Sci. U.S.A. 100*, 6980−6985.
20. Rajagopalan, P. T., and Benkovic, S. J. (2002) Preorganization and protein dynamics in enzyme catalysis, *Chem. Rec. 2*, 24−36.
21. Agarwal, P. K., Billeter, S. R., and Hammes-Schiffer, S. (2002) Nuclear quantum effects and enzyme dynamics in dihydrofolate reductase complexes, *J. Phys. Chem. B 106*, 3283−3293.
22. Kohen, A., and Klinman, J. P. (1998) Enzyme catalysis: Beyond classical paradigms, *Acc. Chem. Res. 31*, 397−404.
23. Kohen, A., and Klinman, J. P. (1999) Hydrogen tunneling in biology, in *Chemistry and Biology* (Schreiber, S. L., and Nicolaou, K. C., Eds.) Vol. 6, pp R191−R198, Elsevier Science, London.
24. Sikorski, R. S., Wang, L., Markham, K. A., Rajagopalan, P. T. R., Benkovic, S. J., and Kohen, A. (2004) Tunneling and coupled motion in the *Escherichia coli* dihydrofolate reductase catalysis, *J. Am. Chem. Soc. 126*, 4778−4779.
25. Knapp, M. J., and Klinman, J. P. (2002) Environmentally coupled hydrogen tunneling: Linking catalysis to dynamics, *Eur. J. Biochem. 269*, 3113−3121.
26. Maglia, G., and Alleman, R. K. (2003) Evidence for environmentally coupled hydrogen tunneling during dihydrofolate reductase catalysis, *J. Am. Chem. Soc. 125*, 13372−13373.
27. Dams, T., Auerbach, G., Bader, G., Jacob, U., Ploom, T., Huber, T., and Jaenicke, R. (2000) The crystal structure of dihydrofolate reductase from *Thermotoga maritime*: Molecular features of thermostability, *J. Mol. Biol. 297*, 659−672.
28. Kohen, A., Cannio, R., Bartolucci, S., and Klinman, J. P. (1999) Enzyme dynamics and hydrogen tunneling in a thermophilic alcohol dehydrogenase, *Nature 399*, 496−499.
29. Kohen, A., and Klinman, J. P. (2000) Protein flexibility correlates with degree of hydrogen tunneling in thermophilic and mesophilic alcohol dehydrogenase, *J. Am. Chem. Soc. 122*, 10738−10739.
30. Liang, Z.-X., Lee, T., Resing, K. A., Ahn, N. G., and Klinman, J. P. (2004) Thermal activated protein mobility and its correlation with catalysis in thermophilic alcohol dehydrogenase, *Proc. Natl. Acad. Sci. U.S.A. 101*, 9556−9561.
31. Liang, Z.-X., Tsigos, I., Lee, T., Bouriotis, V., Resing, K. A., Ahn, N. G., and Klinman, J. P. (2004) Evidence for increased local flexibility in psychrophilic alcohol dehydrogenase relative to its thermophilic homologue, *Biochemistry 43*, 14676−14783.
32. Liang, Z.-X., Tsigos, I., Bouriotis, V., and Klinman, J. P. (2004) Impact of protein parameters in thermophilic and psychrophilic alcohol dehydrogenases, *J. Am. Chem. Soc. 126*, 9500−9501.
33. Blakley, R. L. (1960) Crystalline dihydropteroylglutamic acid, *Nature 188*, 231−232.
34. Jeong, S.-S., and Gready, J. E. (1994) A method of preparation and purification of (4R)-deuterated-reduced nicotinamide adenine dinucleotide phosphate, *Anal. Biochem. 221*, 273−277.

35. Viola, R. E., Cook, P. F., and Cleland, W. W. (1979) Stereoselective preparation of deuterated-reduced nicotinamide adenine nucleotides and substrates by enzymatic synthesis, *Anal. Biochem. 96*, 334−340.
36. Pace, C. N., Vajdos, F., Fee, L., Grimsley, G., and Gray, T. (1995) How to measure and predict the molar absorption coefficient of a protein, *Protein Sci. 4*, 2411−2423.
37. Altschul, S. F., Gish, W., Miller, W., Myers, E. W., and Lipman, D. J. (1990) Basic local alignment search tool, *J. Mol. Biol. 215*, 403−410.
38. Hanahan, D. (1983) Studies on transformation of *Eschericia coli* with plasmids, *J. Mol. Biol. 166*, 557−580.
39. Russell, R. B., and Barton, G. J. (1992) Multiple protein-sequence alignment from tertiary structure comparison: Assignment of global and residue confidence levels, *Proteins 14*, 309−323.
40. Beitz, E. (2000) Texshade: Shading and labeling of multiple sequence alignments using latex, *Bioinformatics 16*, 135−139.
41. Jancarik, J., and Kim, S.-H. (1991) Sparse-matrix sampling: A screening method for crystallization of proteins, *J. Appl. Crystallogr. 24*, 409−411.
42. Vagin, A., and Teplyakov, A. (1997) Molrep: An automated program for molecular replacement, *J. Appl. Crystallogr. 30*, 1022−1025.
43. Brunger, A. T., Adams, P. D., Clore, G. M., Delano, W. L., Gros, P., Grosse-Kunstleve, R. W., Jiang, J. S., Kuszewski, J., Nilges, M., Pannu, N. S., Read, R. J., Rice, L. M., Simonson, T., and Warren, G. L. (1998) Crystallography and NMR system: A new software suite for macromolecular structure determination, *Acta Crystallogr. D54*, 905−921.
44. Jones, T. A., Zhou, J.-Y., Cowan, S. W., and Kjeldgaard, M. (1991) Improved methods for the building of protein models in electron density maps and the location of errors in these models, *Acta Crystallogr. A47*, 110−119.
45. Kraulis, P. J. (1991) Molscript: A program to produce both detailed and schematic plots of protein structures, *J. Appl. Crystallogr. 24*, 946−950.
46. Kabsch, W., and Sander, C. (1983) Dictionary of protein secondary structure: A pattern-recognition of hydrogen-bonded and geometrical features, *Biopolymers 22*, 2577−2637.
47. Laskowski, R. A., MacArthur, M. W., Moss, D., and Thornton, J. M. (1993) Procheck: A program to check the stereochemical quality of protein structures, *J. Appl. Crystallogr. 26*, 283−291.
48. Klinman, J. P., Humphries, H., and Voet, J. G. (1980) Deduction of kinetic mechanism in multisubstrate enzyme reactions from tritium isotope effects: Application to dopamine β-hydroxylase, *J. Biol. Chem. 255*, 11643.
49. Cook, P. F., and Cleland, W. W. (1981) Mechanistic deductions from isotope effects in multireactant enzyme mechanism, *Biochemistry 20*, 1790−1796.
50. Beard, W. A., Appleman, J. R., Delcamp, T. J., Freisheim, J. H., and Blakley, R. L. (1989) Hydride transfer by dihydrofolate reductase. Causes and consequences of the wide range of rates exhibited by bacterial and vertebrate enzymes, *J. Biol. Chem. 264*, 9391−9399.
51. Sawaya, M. R., and Kraut, J. (1997) Loop and subdomain movements in the mechanism of *Escherichia* coli dihydrofolate reductase: Crystallographic evidence, *Biochemistry 36*, 586−603.
52. Davies, J. F., Delcamp, T. J., Prendergast, N. J., Ashford, V. A., Freisheim, J. H., and Kraut, J. (1990) Crystal structures of recombinant human dihydrofolate reductase complexed with folate and 5-deazafolate, *Biochemistry 29*, 9467−9479.
53. Bolin, J. T., Filman, D. J., Matthews, D. A., Hamlin, R. C., and Kraut, J. (1982) Crystal structures of *Escherichia coli* and *Lactobacillus casei* dihydrofolate reductase refined at 1.7 Å resolution. I. General features and binding of methotrexate, *J. Biol. Chem. 257*, 3650−3662.
54. Kitahara, R., Sareth, S., Yamada, H., Ohmae, E., Gekko, K., and Akasaka, K. (2000) High-pressure NMR reveals active site hinge motion of folate bound *Escherichia coli* dihydrofolate reductase, *Biochemistry 39*, 12789−12795.
55. Jaenick, R., and Bohm, G. (1998) The stability of proteins in extreme environments, *Curr. Opin. Struct. Biol. 8*, 738−748.
56. Petsko, G. A. (2001) Structural basis of thermostability in hyperthermophilic proteins, or "there is more than one way to skin a cat", *Methods Enzymol. 334*, 469−478.
57. Van den Burg, B., Vriend, G., Veltman, O., Venema, G., and Eijsink, V. (1998) Engineering an enzyme to resist boiling, *Proc. Natl. Acad. Sci. U.S.A. 95*, 2056−2060.
58. Woltz-Watz, M., Thai, V., Henzler-Wildman, K., Hadjipavlou, G., Eisenmesser, E. Z., and Kern, D. (2004) Linkage between dynamics and catalysis in a thermophilic-mesophilic enzyme pair, *Nat. Struct. Mol. Biol. 11*, 945−949.
59. Hatcher, E., Soudackov, A. V., and Hammes-Schiffer, S. (2004) Proton-coupled electron transfer in soybean lipoxygenase, *J. Am. Chem. Soc. 126*, 5673−5773.
60. Davies, J. F., Matthews, D. A., Oatley, S. J., Kaufman, B. T., Xuong, N.-H., and Kraut, J. Unpublished results.
61. Whitlow, M., Howard, A. J., Stewart, D., Hardman, K. D., Kuyper, L. F., Baccanari, D. P., Fling, M. E., and Tansik, R. L. (1997) X-ray crystallographic studies of *Candida albicans* dihydrofolate reductase. High-resolution structures of the holoenzyme and an inhibited ternary complex, *J. Biol. Chem. 272*, 30289−30298.
62. Champness, J. N., Achari, A., Ballantine, S. P., Bryant, P. K., Delves, C. J., and Stammers, D. K. (1994) The structure of *Pneumocystis carinii* dihydrofolate reductase to 1.9 Å resolution, *Structure 2*, 915−924.
63. Pieper, U., Kapadia, G., Mevarech, M., and Herzberg, O. (1998) Structural features of halophilicity derived from the crystal structure of dihydrofolate reductase from the Dead Sea halophilic archaeon, *Haloferax volcanii*, *Structure 6*, 75−88.
64. Berman, H. M., Westbrook, J., Feng, Z., Gilliland, G., Bhat, T. N., Weissig, H., Shindyalov, I. N., and Bourne, P. E. (2000) The protein data bank, *Nucleic Acids Res. 28*, 235−242.
65. Merritt, E. A., and Murphy, M. E. P. (1994) Raster3D version 2.0: A program for photorealistic molecular graphics, *Acta Crystallogr. D50*, 869−873.

BI050630J